Climatic response to high-latitude volcanic eruptions

Luke Oman, Alan Robock, and Georgiy Stenchikov
Department of Environmental Sciences, Rutgers–State University of New Jersey, New Brunswick, New Jersey, USA

Gavin A. Schmidt[1] and Reto Ruedy[2]
NASA Goddard Institute for Space Studies, New York, New York, USA

Received 4 October 2004; revised 16 February 2005; accepted 21 March 2005; published 1 July 2005.

[1] Strong volcanic eruptions can inject large amounts of SO_2 into the lower stratosphere, which over time, are converted into sulfate aerosols and have the potential to impact climate. Aerosols from tropical volcanic eruptions like the 1991 Mount Pinatubo eruption spread over the entire globe, whereas high-latitude eruptions typically have aerosols which remain in the hemisphere in which they where injected. This causes their largest radiative forcing to be extratropical, and the climate response should be different from that of tropical eruptions. We conducted a 20-member ensemble simulation of the climate response to the Katmai eruption (58°N) of 6 June 1912 using the NASA Goddard Institute for Space Studies ModelE climate model. We also produced an additional 20-member ensemble for a 3 times Katmai (3x Katmai) eruption to see the impact the strength of the eruption has on the radiative as well as the dynamical responses. The results of these simulations do not show a positive Arctic Oscillation response like past simulations of tropical volcanic eruptions, but we did find significant cooling over southern Asia during the boreal winter. The first winter following Katmai and the second winter following 3x Katmai showed strong similarities in lower stratospheric geopotential height anomalies and sea level pressure anomalies, which occurred when the two cases had similar optical depth perturbations. These simulations show that the radiative impact of a high-latitude volcanic eruption was much larger than the dynamical impact at high latitudes. In the boreal summer, however, strong cooling over the Northern Hemisphere landmasses caused a decrease in the Asian monsoon circulation with significant decreases of up to 10% in cloud cover and warming over northern India. Thus the main dynamical impact of high-latitude eruptions is in the summer over Asia.

Citation: Oman, L., A. Robock, G. Stenchikov, G. A. Schmidt, and R. Ruedy (2005), Climatic response to high-latitude volcanic eruptions, *J. Geophys. Res.*, *110*, D13103, doi:10.1029/2004JD005487.

1. Introduction

[2] Volcanic eruptions can inject large amounts of SO_2 into the stratosphere [*Robock*, 2000]. This SO_2 is converted over time into sulfate aerosols which can cause large perturbations to the climate system.

[3] Only a few studies have examined the impact of strong volcanic eruptions outside the tropics. *Graf* [1992] examined the climate perturbations caused by a reduction of incoming solar radiation at high latitudes similar to what would be produced by a volcanic eruption. In those simulations incoming solar radiation was reduced north of 50°N by amounts similar to those produced by the tropical eruption of El Chichón. *Graf and Timmreck* [2001] simulated the aerosol radiative effects of the Laacher See eruption which took place around 10,900 B.C. in Germany. They found that the climatic response was similar to a number of previous studies of tropical eruptions which showed continental winter warming. However, only a single simulation was done for this study, since their main focus was on the radiative impact of the Laacher See eruption. More recently, studies of the Laki fissure series of eruptions, which took place in Iceland in 1783–1784 [*Highwood and Stevenson*, 2003; *Stevenson et al.*, 2003] were conducted by interactively modeling the transport and chemical conversions of the SO_2 gas. They also reported only a slight cooling in the Northern Hemisphere annual mean temperature produced by the Reading Intermediate General Circulation Model (GCM), since their model had most of the aerosols in the troposphere. This likely represents the low end of estimates with other studies suggesting a much higher stratospheric loading [*Thordarson and Self*, 2003].

[4] Most studies have dealt with the effect of recent large tropical eruptions such as the 1982 El Chichón and 1991 Mount Pinatubo eruptions [*Robock*, 2000]. Observations

[1]Also at Center for Climate Systems Research, Columbia University, New York, New York, USA.
[2]Also at SGT Inc., New York, New York, USA.

0148-0227/05/2004JD005487$09.00

[*Robock and Mao*, 1992, 1995] and simulations [*Graf et al.*, 1993; *Kirchner et al.*, 1999; *Stenchikov et al.*, 2002, 2004; *Shindell et al.*, 2004] of tropical eruptions show a pronounced winter warming over the continental Northern Hemisphere. Model simulations from the Geophysical Fluid Dynamics Laboratory (GFDL) SKYHI [*Ramachandran et al.*, 2000; *Stenchikov et al.*, 2002, 2004] and Max Planck ECHAM4 [*Kirchner et al.*, 1999] GCMs have shown that volcanic aerosol heating of the lower stratosphere from thermal infrared (IR) and solar near-IR radiation causes changes in the circulation of the stratosphere by increasing the meridional temperature gradient, resulting in a stronger polar vortex. They also showed that reduced solar radiation in the troposphere caused cooler temperatures in the subtropics, which decreased the meridional temperature gradient. This caused a reduction in the amplitude of planetary waves and allowed further strengthening of the polar vortex. The resulting forced positive phase of the Arctic Oscillation (AO) caused winter warming over the Northern Hemisphere landmasses.

[5] Here we study the impact that high-latitude volcanic eruptions have on climate by examining the Katmai (58°N) eruption of 6 June 1912 as well as an eruption having three times the optical depth of Katmai (3x Katmai). This was done to see the impact the strength of the eruption has on the climate response.

[6] We refer to this eruption as the Katmai eruption, as is commonly done [*Volz*, 1975; *Stothers*, 1996], even though there were eruptions of two nearby volcanoes in Alaska on the same day, Katmai and the larger eruption of Novarupta. Novarupta is located approximately 10 km west of the Katmai volcano, and it was actually responsible for the SO_2 injected into the stratosphere. A large amount of the magma from Novarupta drained from under Katmai which caused the summit of Katmai to collapse forming a caldera more than a kilometer deep [*McGuire and Kilburn*, 1997] An estimated 5 megatons (Mt) of SO_2 was injected into the stratosphere, most of which was confined to north of 30°N [*Stothers*, 1996]. This compares to a stratospheric loading of between 15 to 20 Mt of SO_2 for the Mount Pinatubo eruption [*Bluth et al.*, 1992], although for the Mount Pinatubo eruption the aerosols spread globally. Katmai and Mount Pinatubo produced very similar Northern Hemisphere stratospheric loadings, but Mount Pinatubo put most of its aerosols in the tropics during the first 6 months following the eruption. During the same period nearly all of Katmai's aerosols were extratropical.

[7] Large amounts of SO_2 that are released into the stratosphere convert over time into sulfate aerosols. These sulfate aerosols are primarily heated by outgoing longwave radiation as well as by near-IR solar radiation [*Stenchikov et al.*, 1998]. Since there is less outgoing longwave radiation and solar insolation over the middle and high latitudes, stratospheric aerosols of a high-latitude eruption are heated much less than those over the tropics. Since the majority of aerosols from high-latitude eruptions are extratropical the large seasonal variation of outgoing longwave radiation has a much greater impact on the heating of the stratospheric aerosol layer. However, as the tropics experience very similar temperatures throughout the year this impact is not seen.

[8] *Graf* [1992] noticed in simulating the impact of a high-latitude volcanic eruption by reducing the incoming shortwave radiation north of 50°N that features associated with a weaker Indian monsoon circulation developed. It produced a weakened easterly jet over northern India and anticyclonic vorticity anomalies over the monsoon region. *Graf*'s [1992] results show a positive temperature anomaly over India due to reduced cloudiness and soil moisture from the weakened monsoon.

[9] *Lacis et al.* [1992] found that the two most important factors in determining how volcanic aerosols impact climate forcing are optical depth and effective radius. In the case of Katmai, *Stothers* [2001] showed how the effective radius of Katmai remained smaller than that produced by Mount Pinatubo and was more like the size produced following El Chichón. It is still not completely understood what produces the different effective radius of aerosols following strong volcanic eruptions.

[10] There are two main removal mechanisms for the stratospheric aerosols of a high-latitude volcanic eruption, subsidence over poles and midlatitude troposphere folding. During the winter over the polar regions there is large-scale subsidence which can remove some of the stratospheric aerosols. This process, however, is at most 25% the magnitude of the major removal process which is midlatitude troposphere folding [*Hamill et al.*, 1997].

[11] The goal of this paper is to gain a better understanding of the climatic response of a high-latitude volcanic eruption. In section 2 we briefly describe the Goddard Institute for Space Studies ModelE GCM as well as the design of our experiments. Section 3 examines the radiative impact from our high-latitude volcanic eruption experiments. The results of our modeling simulations are presented in section 4. Section 5 has discussion as well as conclusions from our modeling study.

2. Model Description and Experimental Setup

[12] We used the stratospheric version of the Goddard Institute for Space Studies ModelE GCM for these simulations. It has 23 vertical levels with almost half of them above the tropopause. We used a horizontal resolution of 4° latitude by 5° longitude. This version includes a full gravity wave drag scheme to more accurately model stratospheric processes, which accounts for the effects of gravity waves forming from mountain drag, convection, shear and deformation [*Rind et al.*, 1988]. The radiation scheme uses the correlated k distribution method from *Lacis and Oinas* [1991], which allows implicit representation of absorption and scattering [*Hansen et al.*, 2002] over 33 k intervals in the thermal spectrum. A much more complete overview of this model is given by *Schmidt et al.* [2005].

[13] For this study we used stratospheric aerosol optical depth data from *Ammann et al.* [2003], which have a peak optical depth of 0.3 in September 1912. This is larger than the estimate obtained previously by *Sato et al.* [1993] but agrees better with the *Stothers* [1996, 1997] pyrheliometric data collected from a number of locations [*Volz*, 1975]. These pyrheliometric data were corrected to optical depth at the 0.55 μm wavelength. Since *Ammann et al.* [2003] used a constant effective radius for the sulfate aerosols, we used

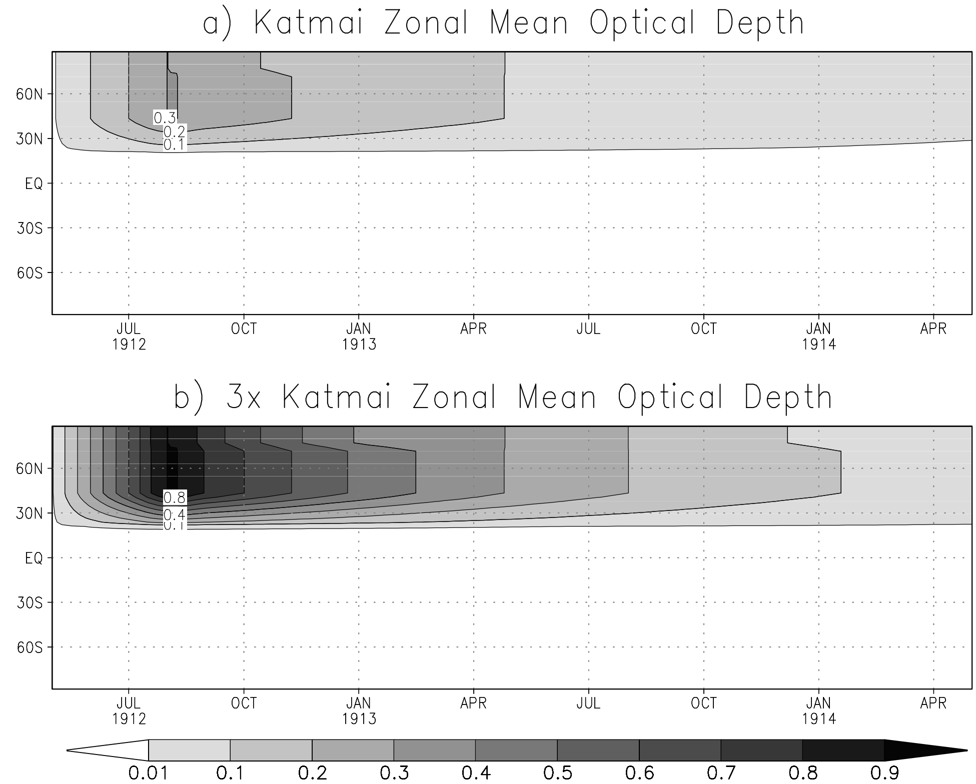

Figure 1. Zonal mean optical depth at the 0.55 μm wavelength used in the model simulation for (a) Katmai and (b) 3x Katmai from May 1912 through May 1914. The aerosol optical depth distribution is from *Ammann et al.* [2003]. See color version of this figure in the HTML.

the *Sato et al.* [1993] estimate for Katmai, which has a variable effective radius and is in better agreement with *Stothers* [1997]. Figure 1 shows the stratospheric optical depth used in our Katmai and 3x Katmai simulations. The peak optical depths are 0.3 and 0.9 in September 1912 for Katmai and 3x Katmai respectively, with the majority of the aerosols north of 30°N latitude.

[14] These simulations were run with the atmosphere-only model using fixed climatological 1946–1955 mean sea surface temperatures and sea ice concentrations [*Rayner et al.*, 2003]. The runs also included estimates of 1913 greenhouse gases and ozone concentrations. 40 years of control run were simulated as well as 20 ensemble members of both the Katmai and 3x Katmai cases. Each ensemble member was integrated for 4 years. To generate the individual ensemble members, we randomly perturbed the initial conditions in selected areas of the troposphere by no more than 1°C for each of the ensemble members. A large number of ensemble members is needed to establish statistical significance at high latitudes due to the high variability in high latitudes.

3. Radiative Impact

[15] Offline calculations of the instantaneous top of atmosphere radiative forcing show a maximum decrease of 9 W/m^2 around August to September 1912 at about 45°N for the Katmai aerosols (Figure 2a) and 27 W/m^2 for the 3x Katmai (Figure 2b) runs. The smaller aerosol loading by the second summer causes a decrease of 3–4 W/m^2 for Katmai and 10–12 W/m^2 for 3x Katmai. The absorption of longwave radiation is largest during the late summer over the midlatitudes, where peak heating of the surface overlaps with high aerosol concentrations, decreasing over time as the aerosol is removed. The net radiative forcing in Figures 2e and 2f shows that reflection plays the dominant role except in the polar night, when the lack of incoming solar radiation causes the absorption of longwave radiation to be greater. This can be best seen in the 3x Katmai case in Figure 2f although the forcing is only 1–2 W/m^2.

[16] The seasonal cycle of radiative forcing is much more apparent for a high-latitude volcanic eruption than for a low-latitude eruption since the aerosols are mostly extra-tropical (Figure 3). The global radiative forcing reaches a seasonal low during boreal winter, and there is not a large contrast between low and high latitudes. This is a feature not seen in past simulations of tropical eruptions since the aerosols typically spread globally [e.g., *Kirchner et al.*, 1999, Figure 1]. The Brewer-Dobson circulation in the stratosphere has a net poleward transport which allows the aerosols from a tropical eruption like Mount Pinatubo to spread globally. This same circulation restricts the equatorward transport of aerosols from Northern Hemisphere high-latitude volcanic eruptions, keeping the majority of the aerosols north of 30°N. Katmai's maximum globally averaged top of atmosphere net radiative forcing of almost −2 W/m^2 compares to Mount Pinatubo's −2.5 W/m^2 [*Kirchner et al.*, 1999]. By examining Northern-Hemi-

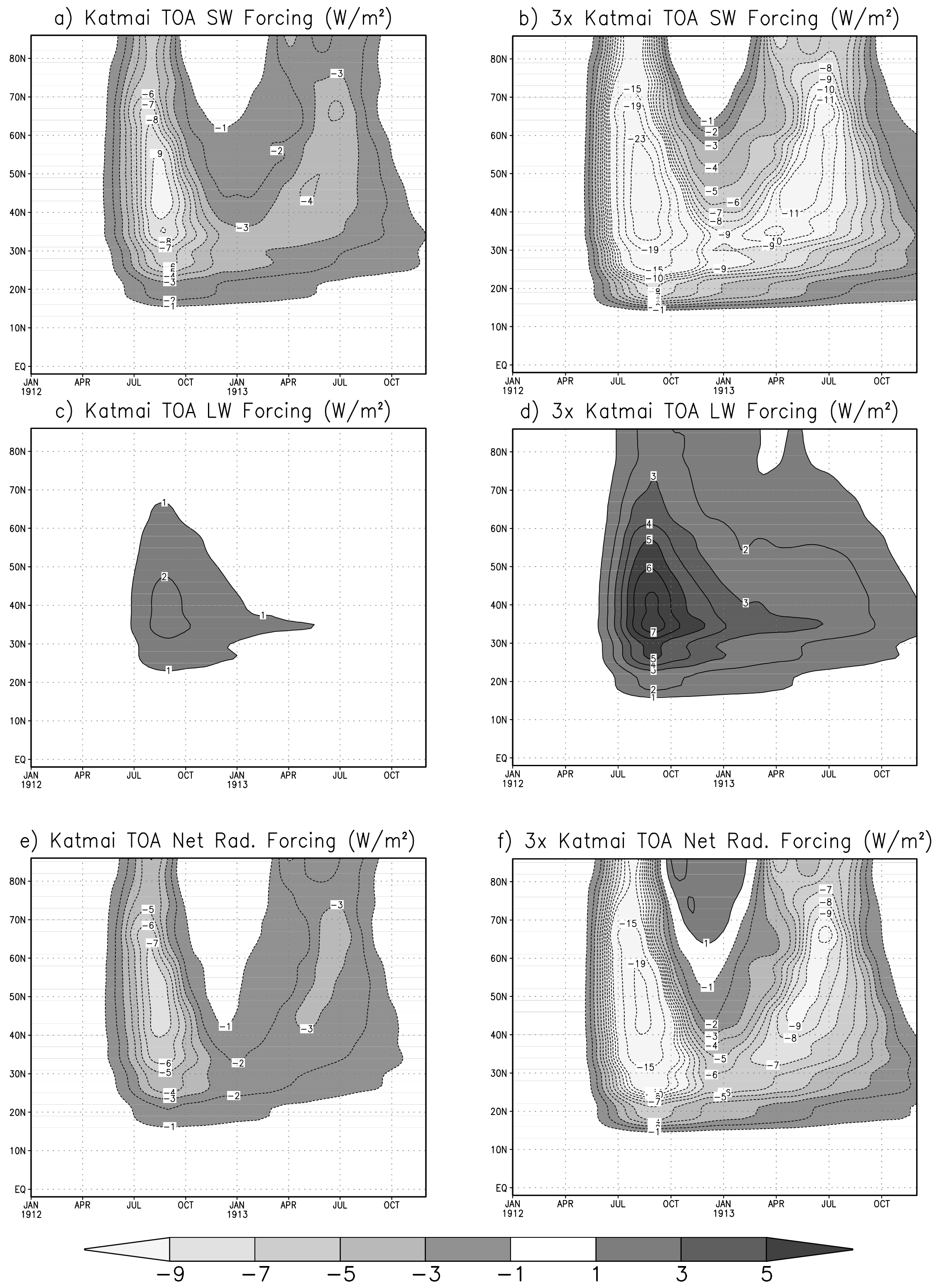

Figure 2. All-sky top of atmosphere (TOA) radiative forcings (W/m^2) calculated for Katmai and 3x Katmai from January 1912 through December 1913 for the Northern Hemisphere. Shown are (a) Katmai TOA shortwave forcing and (b) Katmai TOA longwave forcing, as well as the (c) TOA net radiative forcing for Katmai and (d) TOA shortwave forcing, (e) TOA longwave forcing, and (f) TOA net radiative forcing for 3x Katmai. See color version of this figure in the HTML.

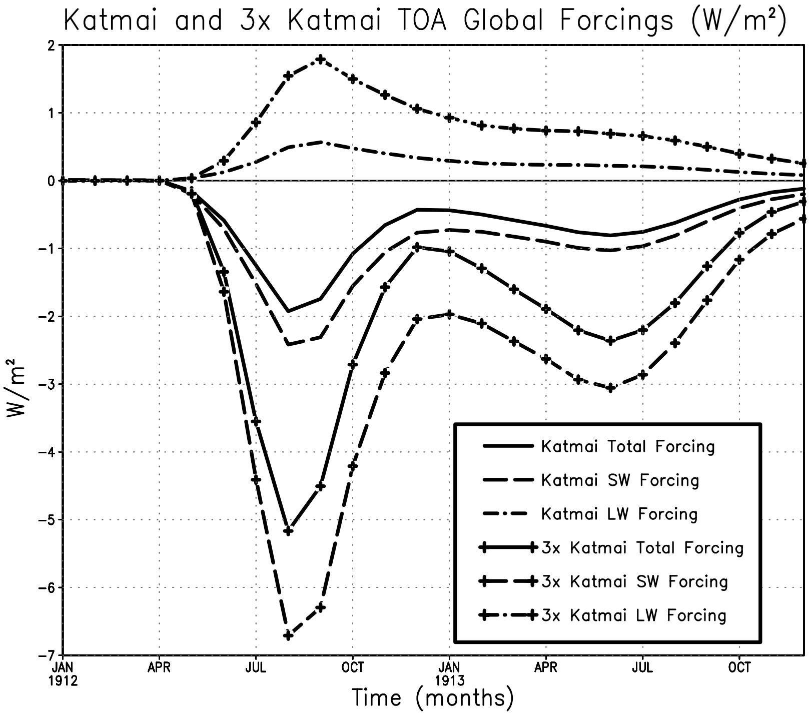

Figure 3. Global average TOA radiative forcings (W/m^2) for Katmai (solid lines) and 3x Katmai (plus marked lines) for January 1912 through December 1913. Solid line indicates the total net radiative forcing, long-dashed line indicates shortwave forcing, and dash-dotted line is for the longwave forcing. Since Katmai aerosols were only in the Northern Hemisphere, doubling the values here would produce the Northern-Hemisphere-only forcing.

sphere-only, Katmai's net radiative forcing of -4 W/m^2 would be larger than that caused by Mount Pinatubo. This is a combined effect of Katmai's larger negative shortwave forcing and smaller positive longwave forcing.

[17] Heating rate anomalies (K/day) for Katmai and 3x Katmai are shown in Figure 4. Figure 4c shows the total heating rate anomaly for Katmai during August 1912. There are 2 main areas of positive heating rate anomalies, which are both over the midlatitudes. The first, between 30 and 150 mbar is the heating (0.1 K/day) of the aerosol layer by outgoing longwave radiation as well as some heating by incoming near-IR [*Stenchikov et al.*, 1998]. The second area is heating of ozone between 5 and 10 mbar and is largely caused by additional upwelling of ultraviolet radiation because of the increased albedo of the sulfate aerosol layer. There is also high-latitude cooling (-0.2 K/day) in the polar stratosphere during August 1912. January 1913 is shown as a typical winter month. The combination of decreased optical depth and less incoming solar and outgoing longwave radiation cause the anomalies to be smaller. One interesting feature that can be most clearly seen in Figure 4h in the 3x Katmai case is that during winter the aerosols are heated from below by outgoing longwave radiation all the way to the polar region while at the same time being cooled from above as the warmer aerosol layer gives off enhanced longwave radiation. The total heating rates from Mount Pinatubo (not shown) over the tropics remain quite similar from August to January following the eruption, whereas, Katmai and 3x Katmai show significant decreases in positive heating rates during that time (Figures 4c, 4d, 4g, and 4h).

4. Results

[18] To establish significance over the middle and high latitudes a larger number of ensemble members needs to be simulated. This is because in general, higher latitudes experience greater climate variability. A total of 20 ensemble member runs were conducted to decrease the effect natural variability has on the climate system and to establish significance at the 95% confidence level.

[19] Figure 5 shows the change in the zonal mean temperature at 70 mbar for Katmai (Figure 5a), 3x Katmai (Figure 5b), and Pinatubo (Figure 5c). The lower stratospheric heating from the Katmai aerosols was a little over 1°C at 30–45°N latitude during the late summer and early part of fall following the eruption. The anomalies decreased during the winter but returned the following summer at about half the previous summer anomalies. Figure 5b shows this a little more clearly in the 3x Katmai case. The simulations showed a 3 to 4°C warming in the late summer/early fall period decreasing to only a 1°C warming during the winter months followed by increased heating during late spring/summer. By contrast results from a Mount Pinatubo simulation conducted with the same model showed no decrease in heating since a large amount of the aerosols was between 30°S and 30°N. This caused a much larger dynamical forcing during the winter than what

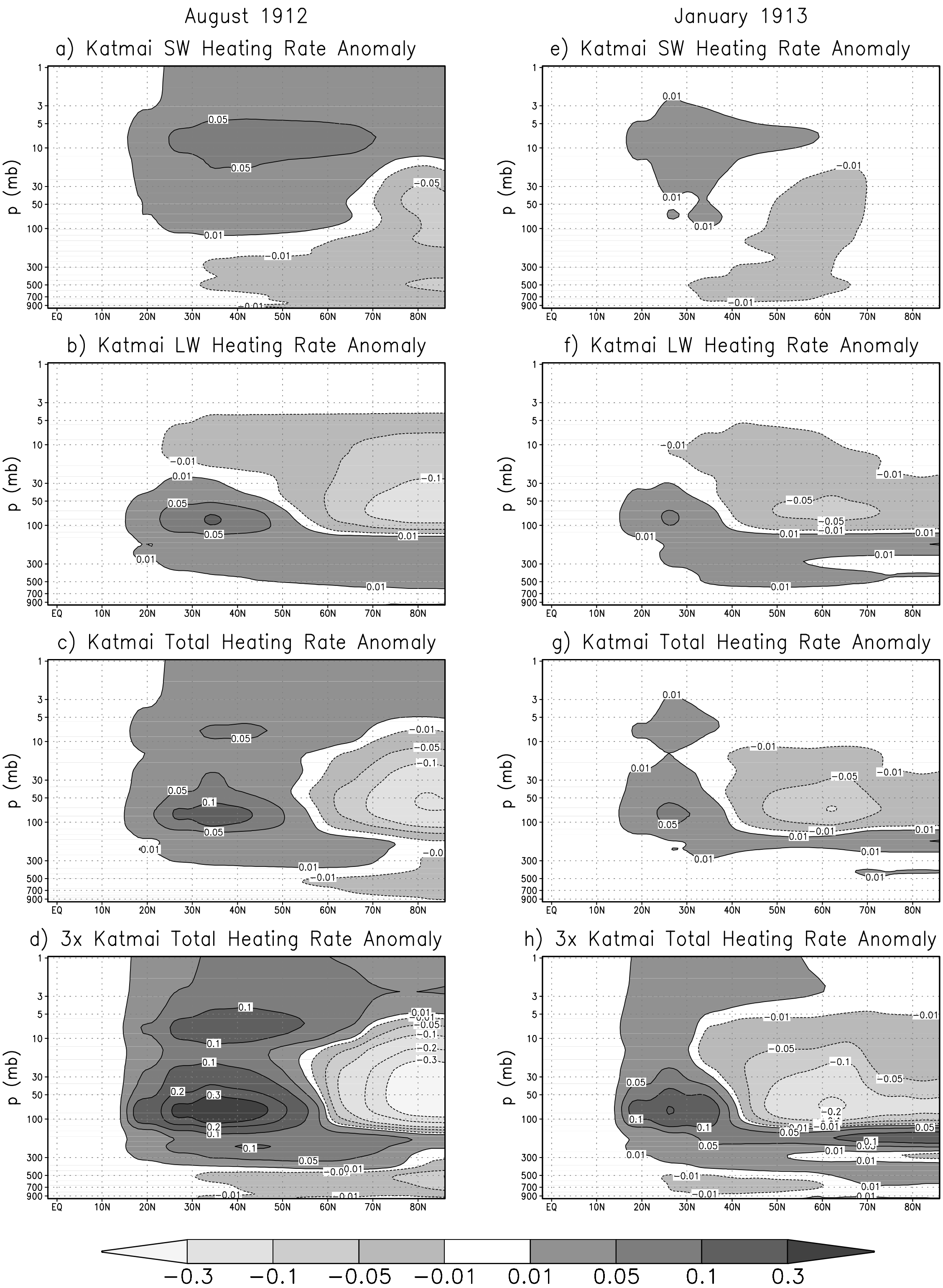

Figure 4. Zonal mean monthly averaged heating rate anomalies (K/day) for (left) August 1912 and (right) January 1913 from the surface to 1 mbar for the Northern Hemisphere. Shown are shortwave heating rate anomalies for (a and e) Katmai, (b and f) longwave heating rate anomalies for Katmai, (c and g) total heating rate anomalies for Katmai, and (d and h) total heating rate anomalies for 3x Katmai. See color version of this figure in the HTML.

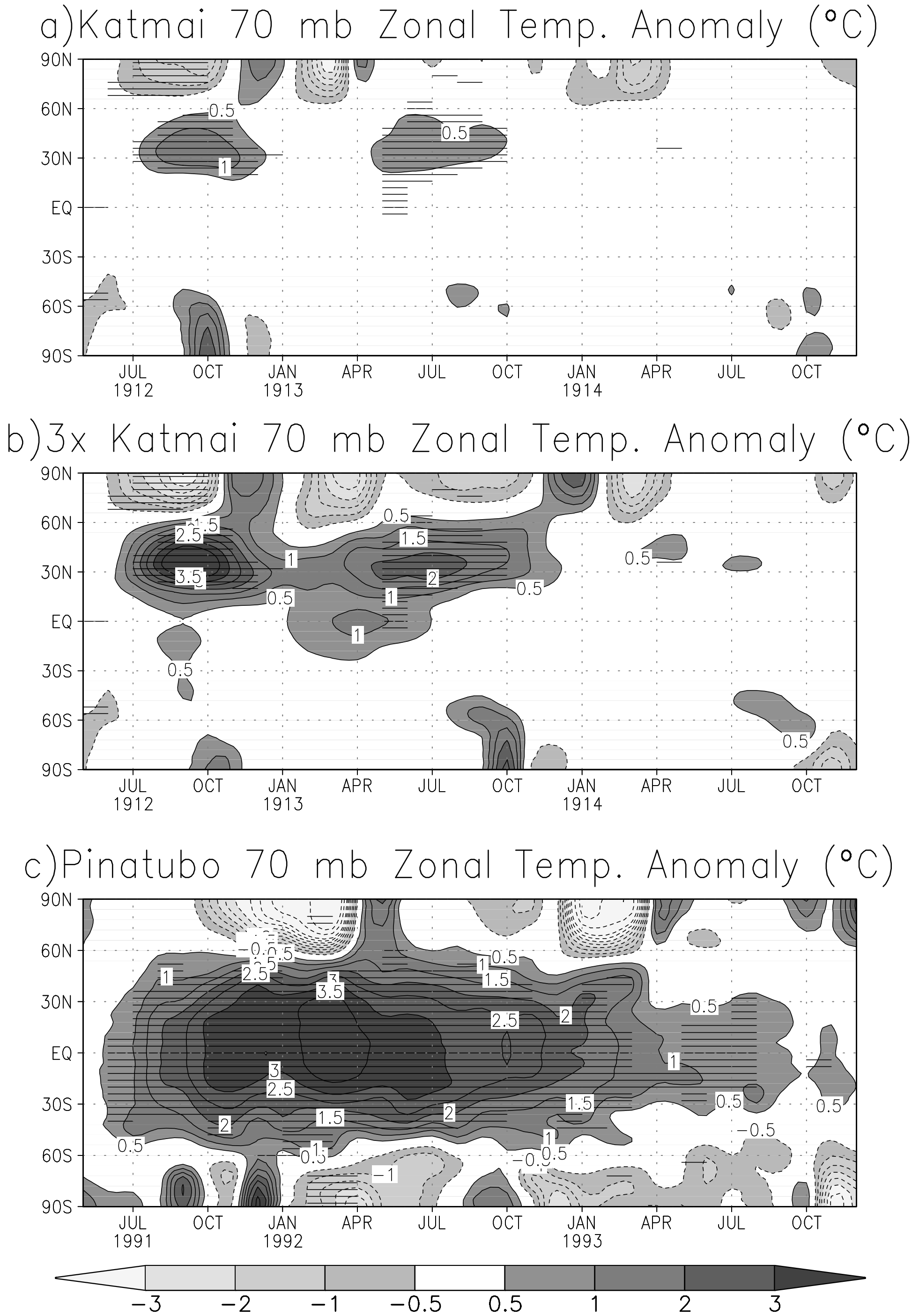

Figure 5. Zonal mean lower stratospheric temperature anomalies (°C) at 70 mbar for 30 months following (a) the Katmai eruption, (b) 3x Katmai, and (c) Pinatubo. The hatching corresponds to a 95% confidence level obtained by a local Student's t test. See color version of this figure in the HTML.

we see from high-latitude volcanic eruptions. The southern extent of significant sulfate aerosols could play a role in determining whether the dynamical forcing remains strong during the Northern Hemisphere winter. Over lower latitudes the heating rates correspond quite well to the lower stratospheric temperature anomalies for Katmai, 3x Katmai, and Mount Pinatubo. However, larger dynamical feedbacks at higher latitudes cause differences between the heating rates and lower stratospheric temperature responses.

[20] The 45 mbar geopotential height (GPH) during the first winter following Katmai increases over the middle and high latitudes (Figure 6a), but only a small portion of it is significant at the 95% confidence level. By the second winter, there is little in the way of significant change to

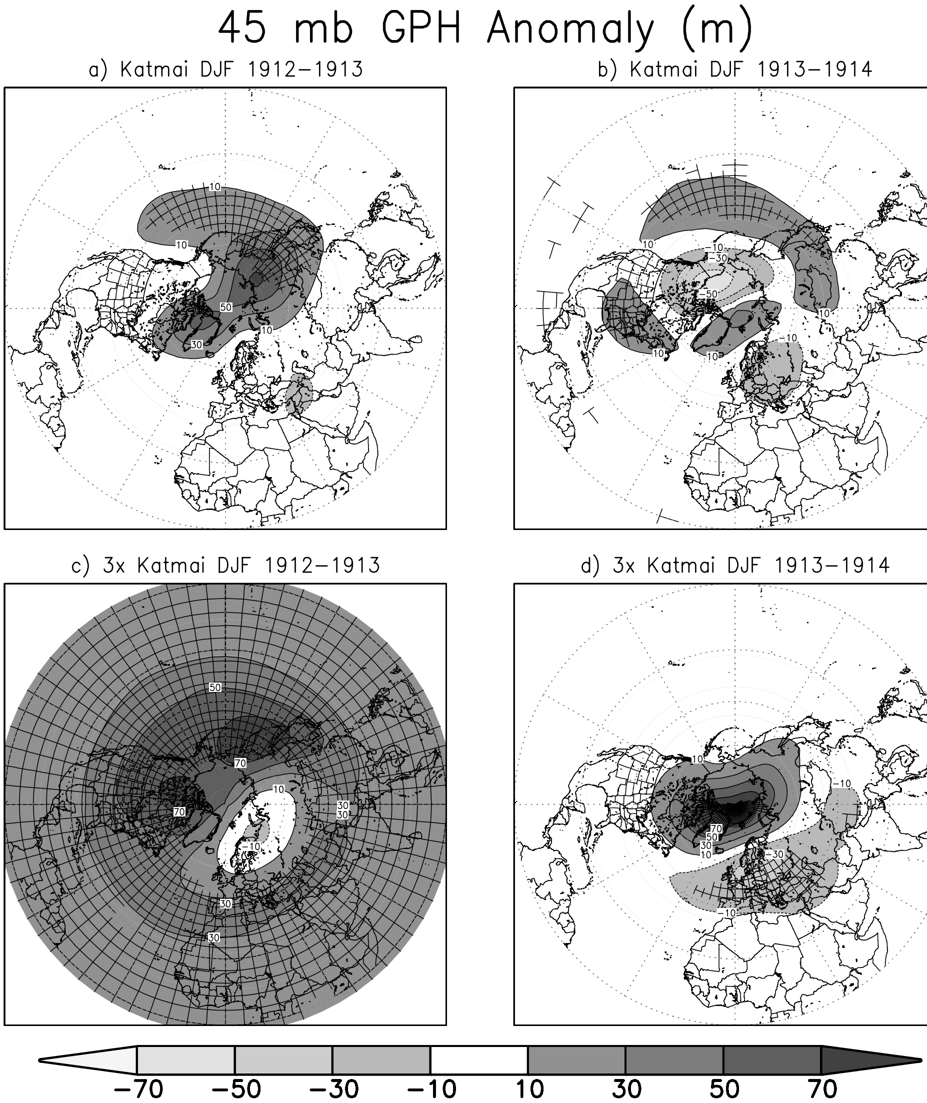

Figure 6. Seasonally averaged geopotential height anomalies (m) at 45 mbar for the (a) first and (b) second winters (DJF) following Katmai and for the (c) first and (b) second winters following 3x Katmai. Anomalies are calculated with respect to 40 years of control runs. The hatching corresponds to a 95% confidence level obtained by a local Student's t test. See color version of this figure in the HTML.

the GPH of the stratosphere (Figure 6b), which is reasonable given that only a small portion of aerosols remain. For the 3x Katmai first winter response (Figure 6c), there is a large area of significance over the low and middle latitudes, with a rather uniform response to stratospheric heating everywhere, but very little over high latitudes with generally positive GPH anomalies. The second winter following the 3x Katmai case (Figure 6d) does have some significant positive GPH anomalies over the high northern latitudes but over a rather small area. These lower stratospheric responses are very different than those of the Pinatubo eruption, which produced negative GPH anomalies over the high latitudes and positive anomalies over the low to middle latitudes causing a positive AO response, as found here and previously [e.g., *Stenchikov et al.*, 2002, 2004; *Shindell et al.*, 2004]. During the winter the positive heating rate anomalies in Figure 4h correspond to positive GPH anomalies in Figure 6c over the low and middle latitudes. In the winter such a relationship is difficult to establish at high latitudes due to the large dynamic variability, but in the summer there is a direct relationship at all latitudes between the heating rate anomalies and the GPH anomalies.

[21] At the surface the temperature response was strongest during summer due to the large radiative impact (Figure 7). Cooling dominates the Northern Hemisphere landmasses especially over Asia, with maximum cooling of about 1 to 1.5°C for the Katmai case and for the 3x Katmai case cooling of up to 2 to 2.5°C during the first summer and 1 to 1.5°C during the second summer but over a significantly larger area.

[22] In contrast to the overall cooling an area of significant warming stands out, especially in Figure 7d, over

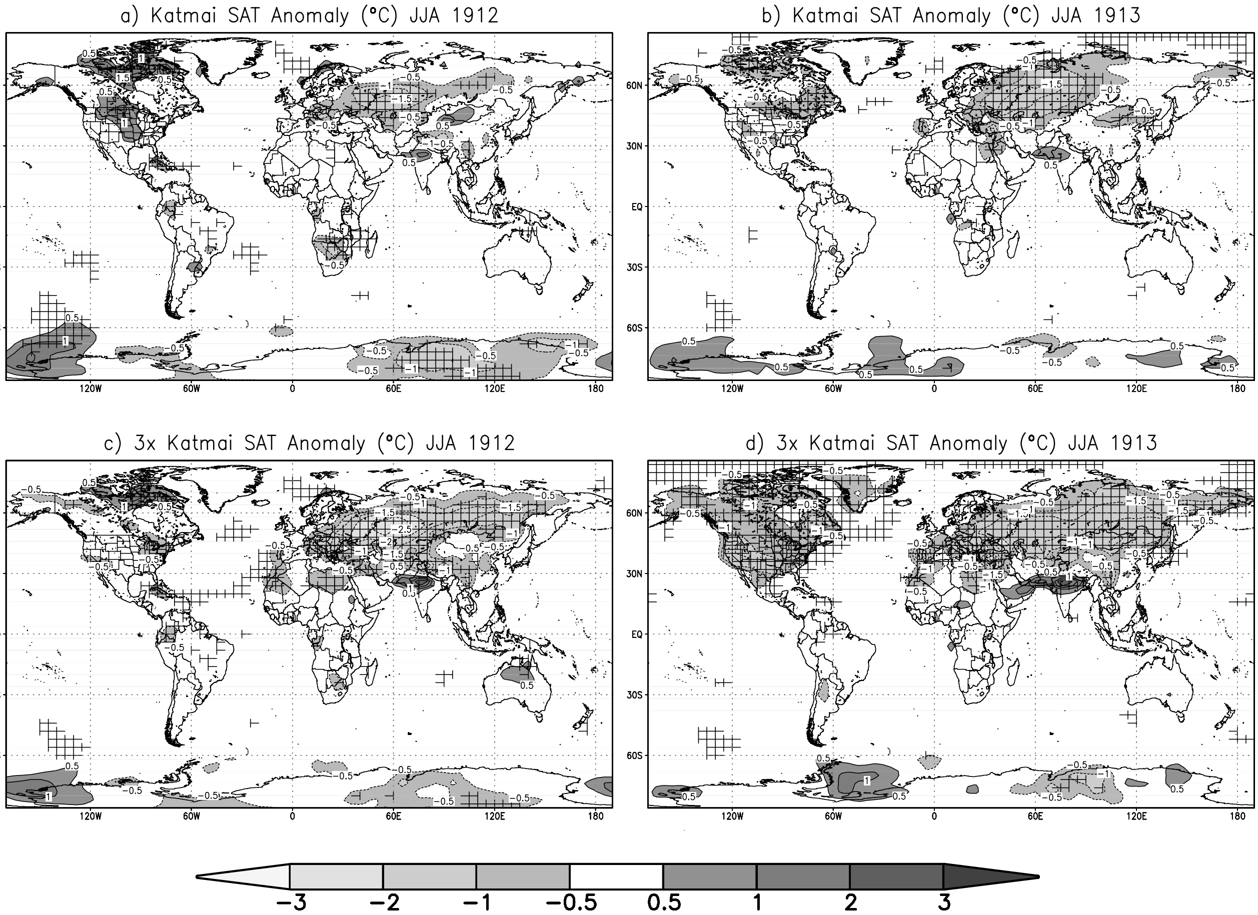

Figure 7. Seasonally averaged surface air temperatures (SAT) anomalies (°C) for the (a) first and (b) second summers (JJA) following Katmai and for the (c) first and (d) second summers following 3x Katmai. Anomalies are calculated with respect to 40 years of control runs. The hatching corresponds to a 95% confidence level obtained by a local Student's t test. See color version of this figure in the HTML.

northern India stretching west to the Persian Gulf. Normally, northern India experiences large amounts of cloudiness and rain due to the monsoon circulation that develops during the summer months, largely driven by the temperature gradient between the Indian Ocean and Asia. The eruption significantly changes this gradient and cloud cover is reduced by up to 10% in this region (Figure 8). *Graf* [1992] also noticed that in his simulations of a high-latitude volcanic eruption, by reducing the shortwave radiation north of 50°N latitude that a weaker monsoon circulation developed as well as a similar warm anomalous region over northern India, due to the decreased cloudiness and soil moisture. In addition we found a significant increase in cloud cover over a large portion of Europe. *Rodwell and Hoskins* [1996] and M. Blackburn (personal communication, 2004) indicated that a weaker monsoon is often associated with increase cloudiness and precipitation over southern Europe.

[23] Figure 9 shows the changes in Northern Hemisphere sea level pressure for Katmai and 3x Katmai in the 2 winters following the eruptions. Generally, higher SLP anomalies occurred over the high latitudes during the first winter following Katmai (Figure 9a) and the second winter following 3x Katmai (Figure 9d), with similar significant decreases over the midlatitude oceanic basins. The significant decrease in pressure over the midlatitude northern Pacific Ocean also occurred in the first winter following the 3x Katmai case although higher SLP anomalies did not result over higher latitudes. These negative SLP anomalies indicate a southward displacement of the Aleutian Low during winter following high-latitude volcanic eruptions. This is consistent with a slight weakening of the polar vortex seen in Figure 6. Figures 6 and 9 show that for lower stratospheric GPH and SLP very similar climatic responses occur in our simulations during the first winter following Katmai and the second winter following 3x Katmai. Since strong volcanic eruptions typically decay in a logarithmic profile with an e-folding time of 11 months these two time periods represent similar atmospheric sulfate loadings. Figure 1 shows that the optical depth for January 1913 for Katmai is approximately 0.15 and for January 1914 for the 3x Katmai case is 0.11. While Figure 9c shows similar features over northern Pacific Ocean as Figure 9a and 9b, they are different over the northern Atlantic Ocean. Since the anomalies in SLP over the northern Atlantic Ocean in

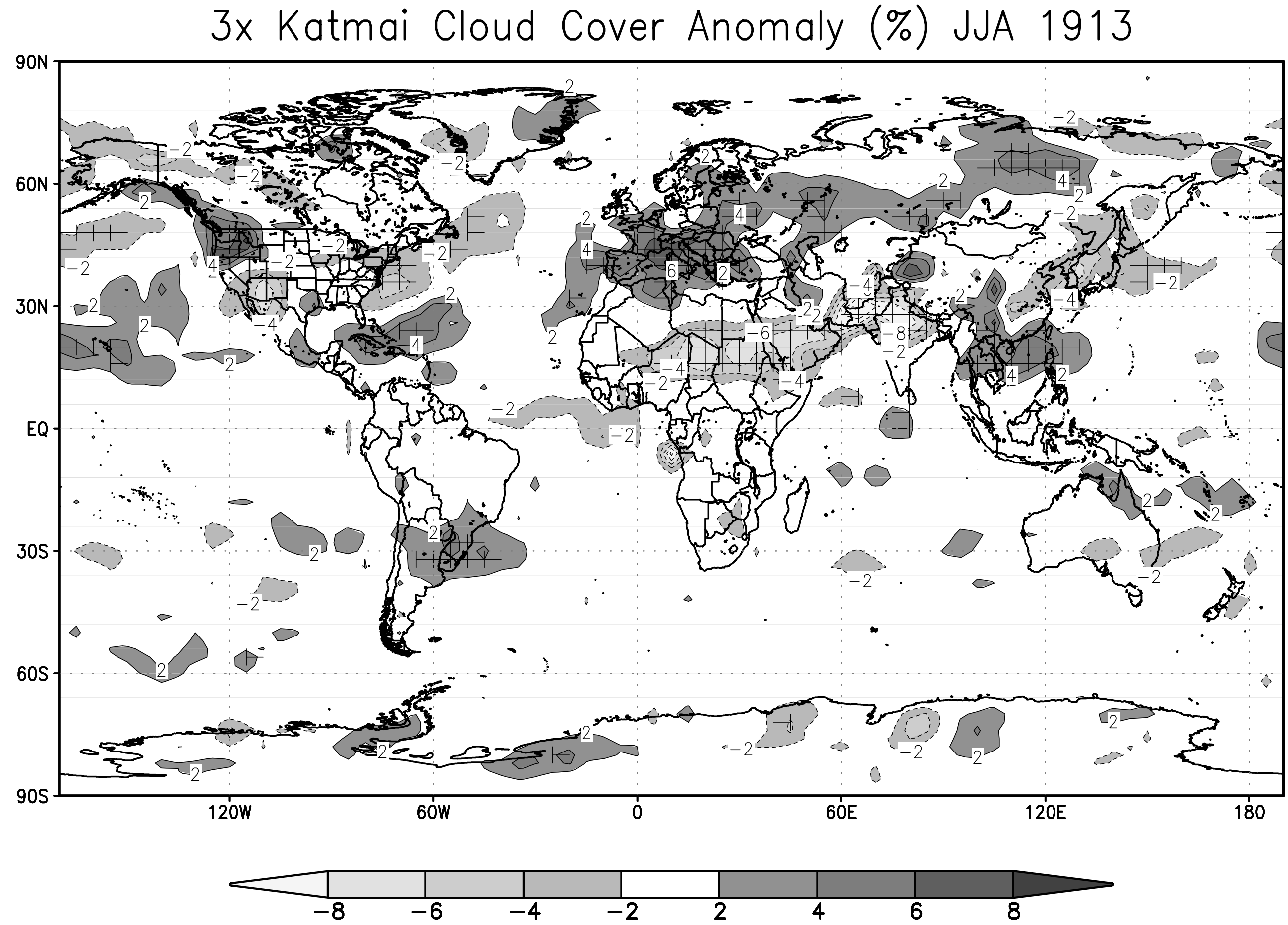

Figure 8. Seasonally averaged anomaly of cloud cover (%) for the second summer (JJA 1913) following the 3x Katmai case. This is the percent change based on 100% cloudiness. Anomalies are calculated with respect to 40 years of control runs. The hatching corresponds to a 95% confidence level obtained by a local Student's t test. See color version of this figure in the HTML.

Figure 9c are not significant it would be difficult to determine the reason. The main point is that even with this much larger forcing during the first winter following 3x Katmai our simulations still do not produce a positive AO response like simulations of past tropical eruptions. During the winter, the only robust surface air temperature changes were cooling over southern Asia in the first winter (Figure 10). The main area of significant cooling over southern Asia is unfortunately in an area that had very few observations during this time period. The few that did exist, however, indicate cooling, though not at a significant level. The higher-latitude patterns are patchy and not typical of positive or negative AO responses. They are much different than the patterns produced in past simulations of tropical eruptions.

5. Discussion and Conclusions

[24] Using the latest member of the Goddard Institute for Space Studies family of GCMs (ModelE), we conducted 20 member ensembles of the Katmai volcanic eruption as well as a 3x Katmai eruption to test the effect the strength of the eruption has on the climate response. We found that both cases look significantly different than past simulations of tropical volcanic eruptions. In the case of Katmai, observations point to most of the aerosols staying north of 30°N latitude. This caused a significant reduction in the heating of the sulfate aerosols especially during winter, and the forcing was not strong enough to cause an enhanced positive AO response as seen in past tropical eruption simulations like Mount Pinatubo. This is the opposite of what was suggested by *Graf and Timmreck* [2001] in which they found a positive AO response in their simulation of the Laacher See eruption. However, since they only conducted one simulation it is difficult to assess a dynamic circulation response, especially at high latitudes during winter, where the large natural variability calls into question the significance of a single simulation. Another difference in their study was that they used the effective radius of sulfate aerosols from the Pinatubo eruption for the Laacher See simulation, which was much larger than the effective radius for Katmai [*Stothers*, 2001].

[25] The main impact from Katmai appears to be the radiative impact, as the dynamical impact appeared to be much weaker. The extent to which the aerosols from a high-latitude eruption reach the tropics could play an important role in the climate response since this could

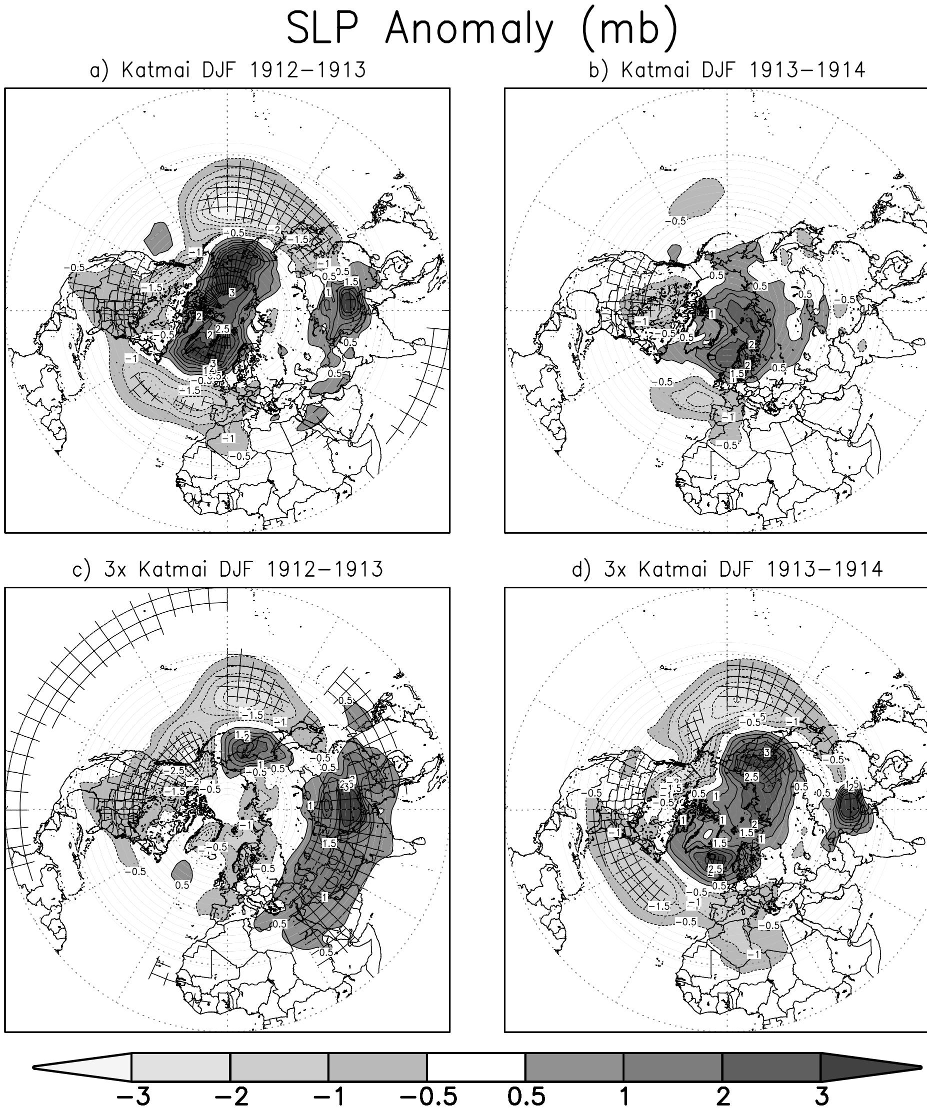

Figure 9. Seasonally averaged sea level pressure (SLP) anomalies (mbar) for the (a) first and (b) second winters (DJF) following Katmai and for the (c) first and (d) second winters following 3x Katmai. Anomalies are calculated with respect to 40 years of control runs. The hatching corresponds to a 95% confidence level obtained by a local Student's t test. See color version of this figure in the HTML.

allow the lower stratospheric heating to remain strong even during the winter.

[26] The first winter following Katmai and the first 2 winters following 3x Katmai all produced significant decreases in SLP over the northern Pacific Ocean. This likely represents a southward displacement of the Aleutian Low during these high-latitude volcanic winters, since similar in magnitude increases in SLP occur to the north. This could be caused by the higher GPH anomalies in Figure 6 which imply a slight weakening of the polar vortex. Also, the first winter following Katmai and second winter following 3x Katmai show remarkably similar responses to SLP and lower stratospheric GPH, these occur at times when the aerosol loading is very similar between the 2 cases. Cooling over southern Asia during winter seems to be a robust response seen in our two high-latitude volcanic cases.

[27] The large radiative cooling over the landmasses during summer in the 3x Katmai case produced a significant reduction in the strength of the Asian monsoon, with warmer temperatures and decreased cloud cover over India. While this feature was evident in the Katmai case the additional strength of the 3x Katmai was necessary to establish statistical significance at the 95% confidence level. These results suggest that future high-latitude eruptions may produce similar effects.

[28] Simulating the Katmai eruption represents the early stages of our work in understanding how high-latitude eruptions impact climate. It is a case that involves a one time injection of SO_2 gas into the lower stratosphere. Future work will examine the Laki fissure series of eruptions in Iceland in 1783–1784, which represent a much more complicated problem. In the case of Laki, 122 Mt of SO_2 gas was injected over 8 months with approximately 19%

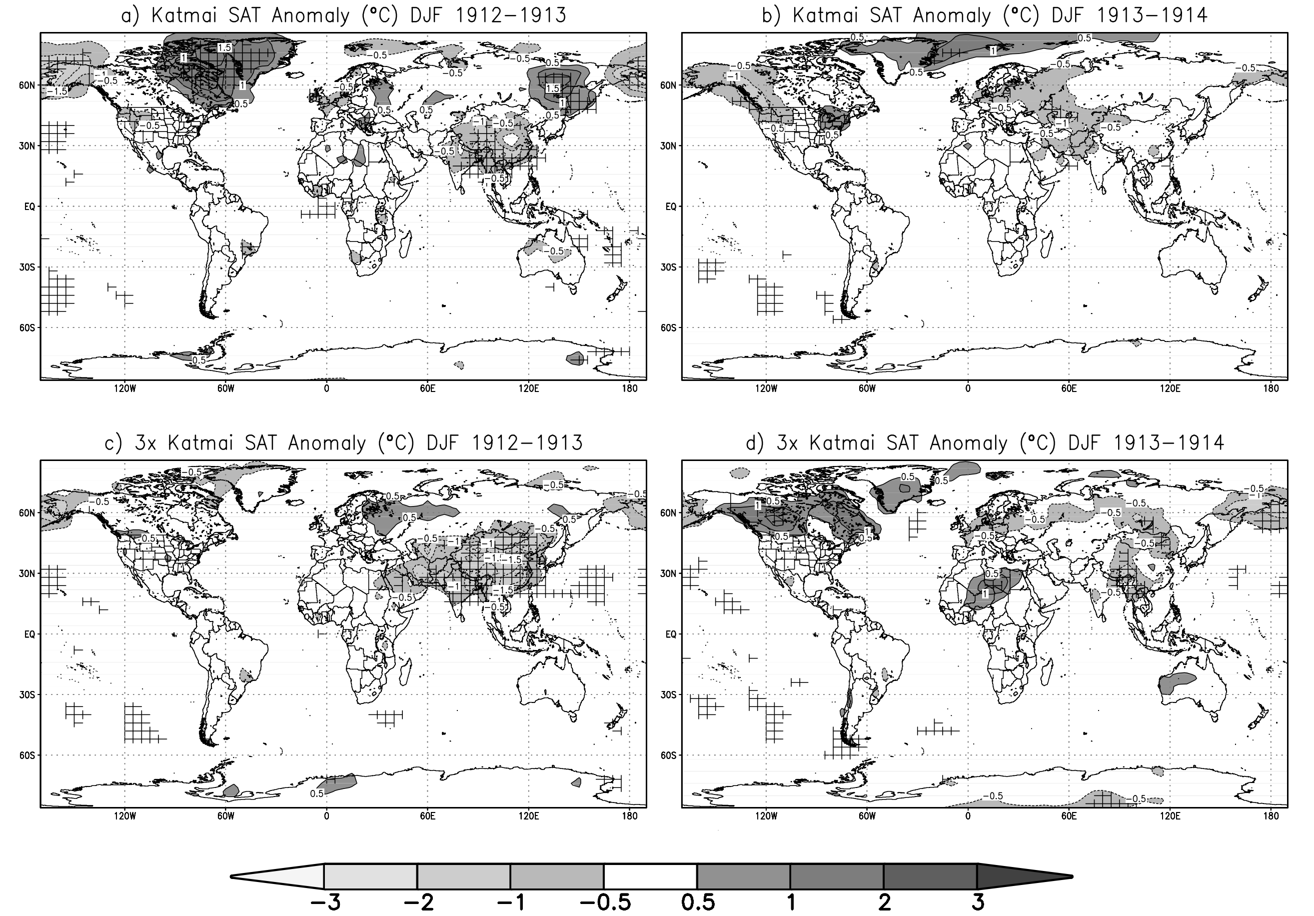

Figure 10. Seasonally averaged surface air temperatures (SAT) anomalies (°C) for the (a) first and (b) second winters (DJF) following Katmai, and for the (c) first and (d) second winters following 3x Katmai. Anomalies are calculated with respect to 40 years of control runs. The hatching corresponds to a 95% confidence level obtained by a local Student's t test. See color version of this figure in the HTML.

confined to the lower troposphere [*Thordarson and Self*, 2003].

[29] **Acknowledgments.** We thank Caspar Ammann for his volcanic aerosol data set and the reviewers for their helpful comments. Luke Oman is supported by a Graduate Assistantship in Areas of National Need fellowship, and this work is supported by NSF grant ATM-0313592. Model development at GISS is supported by NASA climate modeling grants.

References

Ammann, C. M., G. A. Meehl, W. M. Washington, and C. S. Zender (2003), A monthly and latitudinally varying volcanic forcing dataset in simulations of 20th century climate, *Geophys. Res. Lett.*, *30*(12), 1657, doi:10.1029/2003GL016875.

Bluth, G. J. S., S. D. Doiron, A. J. Krueger, L. S. Walter, and C. C. Schnetzler (1992), Global tracking of the SO_2 clouds from the June 1991 Mount Pinatubo eruptions, *Geophys. Res. Lett.*, *19*, 151–154.

Graf, H.-F. (1992), Arctic radiation deficit and climate variability, *Climate Dyn.*, *7*, 19–28.

Graf, H.-F., and C. Timmreck (2001), A general climate model simulation of the aerosol radiative effects of the Laacher See eruption, *J. Geophys. Res.*, *106*, 14,747–14,756.

Graf, H.-F., I. Kirchner, A. Robock, and I. Schult (1993), Pinatubo eruption winter climate effects: Model versus observations, *Clim. Dyn.*, *9*, 81–93.

Hamill, P., E. J. Jensen, P. B. Russell, and J. J. Bauman (1997), The life cycle of stratospheric aerosol particles, *Bull. Am. Meteorol. Soc.*, *78*, 1395–1410.

Hansen, J., et al. (2002), Climate forcings in Goddard Institute for Space Studies SI2 000 simulations, *J. Geophys. Res.*, *107*(D18), 4347, doi:10.1029/2001JD001143.

Highwood, E. J., and D. S. Stevenson (2003), Atmospheric impact of the 1783–1784 Laki eruption: Part II Climatic effect of sulphate aerosol, *Atmos. Chem. Phys. Discuss.*, *3*, 1599–1629.

Kirchner, I., G. L. Stenchikov, H.-F. Graf, A. Robock, and J. C. Antuña (1999), Climate model simulation of winter warming and summer cooling following the 1991 Mount Pinatubo volcanic eruption, *J. Geophys. Res.*, *104*, 19,039–19,055.

Lacis, A., and V. Oinas (1991), A description of the correlated k-distribution method for modeling nongray gaseous absorption, thermal emission, and multiple scattering in vertically inhomogeneous atmospheres, *J. Geophys. Res.*, *96*, 9027–9063.

Lacis, A., J. Hansen, and M. Sato (1992), Climate forcing by stratospheric aerosols, *Geophys. Res. Lett.*, *19*, 1607–1610.

McGuire, B., and C. Kilburn (1997), *Volcanoes of the World*, 144 pp., Kiln House, London.

Ramachandran, S., V. Ramaswamy, G. L. Stenchikov, and A. Robock (2000), Radiative impacts of the Mount Pinatubo volcanic eruption: Lower stratospheric response, *J. Geophys. Res.*, *105*, 24,409–24,429.

Rayner, N. A., D. E. Parker, E. B. Horton, C. K. Folland, L. V. Alexander, D. P. Rowell, E. C. Kent, and A. Kaplan (2003), Global analyses of sea surface temperature, sea ice, and night marine air temperature since the late nineteenth century, *J. Geophys. Res.*, *108*(D14), 4407, doi:10.1029/2002JD002670.

Rind, D., R. Suozzo, N. Balachandran, A. Lacis, and G. Russell (1988), The GISS Global Climate-Middle Atmosphere Model. Part I: Model structure and climatology, *J. Atmos. Sci.*, *45*, 329–370.

Robock, A. (2000), Volcanic eruptions and climate, *Rev. Geophys.*, *38*, 191–219.

Robock, A., and J. Mao (1992), Winter warming from large volcanic eruptions, *Geophys. Res. Lett.*, *12*, 2405–2408.

Robock, A., and J. Mao (1995), The volcanic signal in surface temperature observations, *J. Clim.*, *8*, 1086–1103.
Rodwell, M. J., and B. J. Hoskins (1996), Monsoons and the dynamics of deserts, *Q. J. R. Meteorol. Soc.*, *122*, 1385–1404.
Sato, M., J. E. Hansen, M. P. McCormick, and J. B. Pollack (1993), Stratospheric aerosol optical depths, 1850–1990, *J. Geophys. Res.*, *98*, 22,987–22,994.
Schmidt, G. A., et al. (2005), Present day atmospheric simulations using GISS ModelE: Comparison to in-situ, satellite and reanalysis data, *J. Clim.*, in press.
Shindell, D. T., G. A. Schmidt, M. E. Mann, and G. Faluvegi (2004), Dynamic winter climate response to large tropical volcanic eruptions since 1600, *J. Geophys. Res.*, *109*, D05104, doi:10.1029/2003JD004151.
Stenchikov, G. L., I. Kirchner, A. Robock, H.-F. Graf, J. C. Antuña, R. G. Grainger, A. Lambert, and L. Thomason (1998), Radiative forcing from the 1991 Mount Pinatubo volcanic eruption, *J. Geophys. Res.*, *103*, 13,837–13,857.
Stenchikov, G. L., A. Robock, V. Ramaswamy, M. D. Schwarzkopf, K. Hamilton, and S. Ramachandran (2002), Arctic Oscillation response to the 1991 Mount Pinatubo eruption: Effects of volcanic aerosols and ozone depletion, *J. Geophys. Res.*, *107*(D24), 4803, doi:10.1029/2002JD002090.
Stenchikov, G., K. Hamilton, A. Robock, V. Ramaswamy, and M. D. Schwarzkopf (2004), Arctic Oscillation response to the 1991 Pinatubo eruption in the SKYHI GCM with a realistic Quasi-Biennial Oscillation, *J. Geophys. Res.*, *109*, D03112, doi:10.1029/2003JD003699.
Stevenson, D. S., C. E. Johnson, E. J. Highwood, V. Gauci, W. J. Collins, and R. G. Derwent (2003), Atmospheric impact of the 1783–1784 Laki eruption: Part I Chemistry modeling, *Atmos. Chem. Phys. Discuss.*, *3*, 551–596.
Stothers, R. B. (1996), Major optical depth perturbations to the stratosphere from volcanic eruptions: Pyrheliometric period, 1881–1960, *J. Geophys. Res.*, *101*, 3901–3920.
Stothers, R. B. (1997), Stratospheric aerosol clouds due to very large volcanic eruptions of the early twentieth century: Effective particle sizes and conversion from pyrheliometric to visual optical depth, *J. Geophys. Res.*, *102*, 6143–6151.
Stothers, R. B. (2001), A chronology of annual mean effective radii of stratospheric aerosols from volcanic eruptions during the twentieth century as derived from ground-based spectral extinction measurements, *J. Geophys. Res.*, *106*, 32,043–32,049.
Thordarson, T., and S. Self (2003), Atmospheric and environmental effects of the 1783–1784 Laki eruption: A review and reassessment, *J. Geophys. Res.*, *108*(D1), 4011, doi:10.1029/2001JD002042.
Volz, F. E. (1975), Distribution of turbidity after the 1912 Katmai eruption in Alaska, *J. Geophys. Res.*, *80*, 2643–2648.

L. Oman, A. Robock, and G. Stenchikov, Department of Environmental Sciences, Rutgers–State University of New Jersey, 14 College Farm Road, New Brunswick, NJ 08901-8551, USA. (oman@cep.rutgers.edu)
R. Ruedy and G. A. Schmidt, NASA Goddard Institute for Space Studies, New York, NY 10025, USA.